Indian Journal of Pure & Applied Physics
Vol. 64, February 2026, pp. 133-139
DOI: 10.56042/ijpap.v64i2.21426

A Refined Grodzins Based Signature for Shape Phase Transitions in Rare Earth Nuclei Using the Interacting Boson Approximation

Mudasir Ahmad & Amit Bindra*
Department of Physics, School of Chemical Engineering and Physical Science, Lovely Professional University, Jalandhar 144 411, India

Received: 9th July 2025; accepted: 5th January 2026

This study investigates a refined empirical signature, the Grodzins systematics expressed as dE4/2 ×B(E2; $0^+ \rightarrow 2^+$) within the framework of the Interacting Boson Approximation (IBA), focusing on its correlation to the control parameter (ζ) and its role in nuclear shape transitions. By analyzing even-even nuclei with Z < 76, N = 86–102, a critical transition point is identified near $\zeta \approx 0.6$, corresponding to the boundary between spherical U(5) and deformed SU(3)/γ-soft O(6) regimes, where rapid changes in collectivity and excitation systematics occur. This critical value corresponds to the point where quadrupole–quadrupole correlations begin to dominate over single-boson dynamics, leading to abrupt changes in excitation energy ratios and electromagnetic collectivity, as supported by abrupt shifts in R6/0 energy ratios and B(E2; $0^+ \rightarrow 2^+$) transition probabilities. Notable anomalies around N ~ 90-100, suggest the onset of shape coexistence. This approach offers a sensitive diagnostic for nuclear collectivity and shape transitions without invoking model-dependent assumptions.

Keywords: Collectivity, Interacting boson approximation (IBA), Nuclear structure, Shape transition

1 Introduction

The role of inter-nucleon interaction in driving quantum shape transitions (QST) in stable nuclei has long been emphasized[1, 2]. The development of critical point symmetries (CPS) as a new class of empirically validated models[3,4] has spurred extensive experimental efforts[5-7] to identify nuclei aligning with CPS principles. Notably symmetries like X(5) and E(5), which illustrate first- and second-order phase transitions, respectively, between vibrational and rotational regimes, have received substantial support from both theory and experiment[3, 8–10].

The density of d-bosons (n_d) in both the excited 0^+ state and the ground state, along with the isomeric displacement between the 2^+ state and the 0^+ states, has been theoretically predicted[11]. These studies revealed significant variations in these quantities across transitional regions, exhibiting clear trends associated with nuclear shape evolution, particularly in systems with limited boson numbers (N_B). In a related analysis, the B4/2 ratio (i.e B(E2; $4^+ \rightarrow 2^+$)/B(E2; $2^+ \rightarrow 0^+$)) and observed a distinct peak preceding the U(5)-SU(3) transition[12], consistent with trends in d-boson densities.

Persistent structural differences between the U(5)–SU(3) and U(5)–O(6) transitions have been highlighted through analyses[13] of excitation energy ratios and electromagnetic transition strengths for systems with boson numbers up to $N_B = 50$. However, precise experimental determination of these observables remains challenging for exotic nuclei, often leading to substantial uncertainties. Moreover, the B4/2 ratio typically exhibits only marginal variation (in the range 1.4–1.7), thereby limiting its effectiveness as a sensitive diagnostic observable.

In contrast, excitation energies and two-neutron separation energies across rare-earth nuclei in the region Gd–Hf (N = 86–104) have been investigated using a modified IBA-1 Hamiltonian, revealing bifurcated structural behavior[14]. In particular, isotopes from Yb to Hf exhibit notable deviations from standard systematics, primarily attributable to the enhanced role of the 0_2^+ state. Furthermore, the $R_{6/0}$ ratio (= $E(6_1^+)/E(0_2^+)$) has been shown to serve as a robust probe of nuclear shape transitions in Nd–Dy isotopes, characteristic of first-order quantum phase transitions[15].

More recently, an empirical framework linking the Grodzins product with the P-factor has been introduced to investigate nuclear deformation systematics[16–18]. This approach has subsequently been refined through the development of a compact analytical expression capable of capturing subtle sub-shell effects and structural transformations[19]. In a related context, first-order phase transitions across the Se, Zr, Mo, and Nd isotopic chains have been identified[20] through analyses

*Corresponding author: E-mail: amit.16041@lpu.co.in

of microscopic shape evolution in regions near neutron numbers N = 40, 60, and 90.

In light of these advancements, the present study proposes a new empirical signature $dE_{4/2} \times B(E2; 0^+ \rightarrow 2^+)$—as a dynamic and intuitive indicator of nuclear shape transitions. When examined in conjunction with the ζ parameter of the IBA model, this signature reveals critical structural features across isotopic chains and provides a powerful diagnostic tool for probing nuclear collectivity and phase coexistence in rare-earth nuclei.

2 Theory

Understanding the dynamic behavior of atomic nuclei composed of a finite number of protons and neutrons — requires a comprehensive examination of systematic changes in observable properties, particularly those occurring near critical points. The Sm isotopic chain has been extensively investigated, demonstrating that the Interacting Boson Model (IBM) can successfully reproduce diverse nuclear configurations using a relatively simple Hamiltonian[21]. The inherent flexibility of the IBM allows it to describe a broad spectrum of nuclear phenomena.

This study explores the transition from spherical to deformed nuclear configurations through a simplified two-parameter Hamiltonian. Comprehensive calculations were carried out across several rare-earth isotopic chains, accompanied by a detailed analysis of the resulting parameters and observables to gain deeper insights into structural transformations. These computations were performed using the Extended Consistent- Q Formalism (ECQF)[22], combined with the Hamiltonian formulation introduced[23, 24] within the IBA framework:

$$H = g[(1 - \zeta)\, n_d - \zeta \cdot Q.Q/4N_B] \quad \ldots (1)$$

Here, $n_d = d^\dagger \cdot \tilde{d}$ is the d-boson number operator, and $Q = (s^\dagger \tilde{d} + d^\dagger s) + \chi\, (d^\dagger \tilde{d})^{(2)}$ represents the quadrupole operator. Here, N_B denotes the number of valence bosons, and g is a scalar strength parameter. The Hamiltonian is scaled such that g has units of energy.

The Hamiltonian contains two (unit less) key variables: χ ranging from 0 to -1.32 and ζ ranging from 0 to 1. Physically, the control parameter ζ regulates the competition between the single d-boson energy term and the quadrupole–quadrupole interaction. As ζ increases, collective correlations strengthen, driving the nucleus from spherical vibrational behavior toward axially deformed or γ-soft configurations. The rapid structural changes observed near $\zeta \approx 0.6$ signal a critical balance between these competing degrees of freedom. These parameters define three limiting dynamical symmetries within the IBA model

i U(5), where ζ = 0 for any χ value,
ii SU(3), where χ = -1.32 and ζ = 1.0,
iii O(6), characterized by χ = 0.0 and ζ = 1.0.

All calculations were carried out using the IBAR code[25] and the resulting parameters were used to generate a full depiction of the isotopic sequences within the IBA parameter space. This depiction is shown as the IBA symmetry triangle (Fig. 1).

Even-even nuclei in the rare-earth region—spanning Z=64–72 and N=86–102—are examined using available experimental data compiled in the literature[14] and the Evaluated Nuclear Structure Data File (ENSDF)[26]. Figure 2 provides a synopsis of key findings across these nuclei, focusing on the variation of ζ as a function of mass number A, while Tables 1 and 2 offer a more detailed analysis of the extracted parameters.

In general, an increase in valence bosons correlates with a rising ζ value, indicating a gradual evolution from vibrational to rotational nuclear behavior. This trend is consistently observed across most isotopic chains up to N=92. However, beyond N=92, Gd, Dy, and Er exhibit continued increases in ζ, whereas Yb and Hf maintain comparatively stable ζ values until reaching the mid-shell region.

2.1 Calculations

We utilize the following relationships

$$E4/2 = E41^+/E^+ \quad \ldots (2)$$

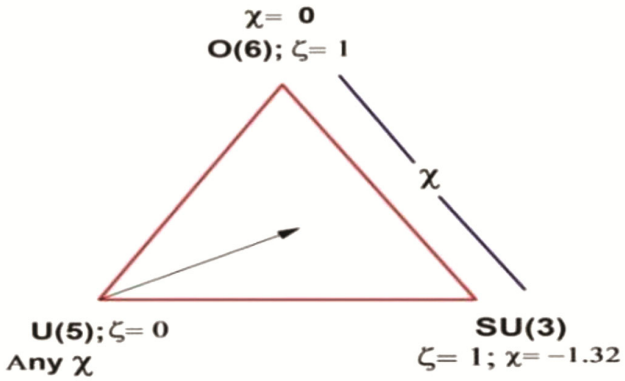

Fig. 1 — The formualtion of the Hamiltonian, as outlined in Eq. (1), simplifies the representation of the IBA symmetry triangle while maintaining consistent boundary conditions for U(5), SU(3) and O(6)

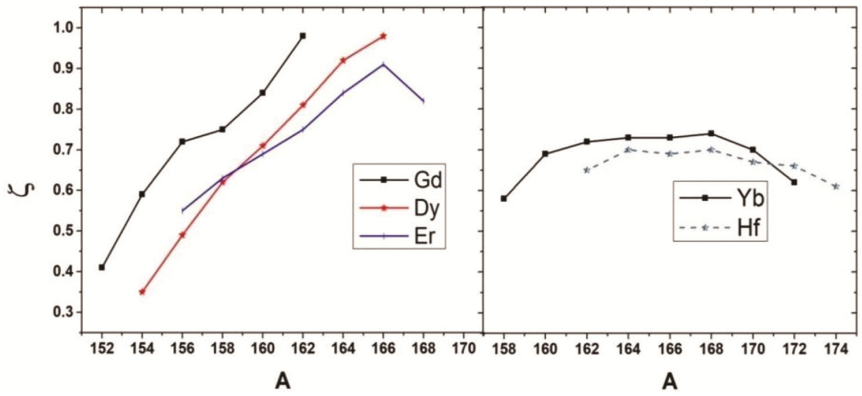

Fig. 2 — Even–even rare-earth nuclei ($64 \le Z \le 72$) exhibit a systematic evolution of the control parameter ζ with mass number. A sharp U(5) → SU(3) shape transition occurs near $\zeta_{crit} \approx 0.6$, particularly for $N \le 92$. Phase coexistence is indicated in ^{170}Yb (N =100), suggesting a mid-shell anomaly

Table 1 — Calculated parameters of the first excited 0^+ states in transitional rare-earth isotopes. A systematic decrease of $E0_2^+$ energy from Gd to Er with increasing ζ, most pronounced for N > 90, is observed, consistent[15]. Energies[27] and B(E2) values[28]

Nuclei	N	A	NB	ε=2(NB-1)A [29] (keV)	k (keV)	ε/ k = 4NB (1- ζ)/ ζ	ζ = 4NB/(ε/ k)+4NB[24]	(dE4/2*B(E2)↑); e^2b^2
64Gd	88	152	10	2736	47.53	57.56	0.41	1.3571
64Gd	90	154	11	3080	100.75	30.57	0.59	0.8712
64Gd	92	156	12	3432	200.58	17.11	0.72	0.2303
64Gd	94	158	13	3792	237.00	16.00	0.75	0.0661
64Gd	96	160	14	4160	420.20	9.90	0.84	0
64Gd	98	162	15	4536	3978.94	1.14	0.98	-0.0385
66Dy	86	154	10	2772	41.46	66.85	0.35	0.1190
66Dy	88	156	11	3120	74.94	41.63	0.49	1.6940
66Dy	90	158	12	3476	116.02	26.96	0.62	1.0155
66Dy	92	160	13	3840	195.91	19.60	0.71	0.2982
66Dy	94	162	14	4212	345.52	12.19	0.81	0.1161
66Dy	96	164	15	4592	944.85	4.86	0.92	0.03871
66Dy	98	166	16	5312	4354.09	1.22	0.98	0.0560
68Er	88	156	10	2808	95.34	29.45	0.55	0.7057
68Er	90	158	11	3160	134.52	23.49	0.63	1.2270
68Er	92	160	12	3520	178.13	19.76	0.69	0.5511
68Er	94	162	13	3888	243.00	16.00	0.75	0.2318
68Er	96	164	14	4264	430.70	9.90	0.84	0.0654
68Er	98	166	15	4648	840.50	5.53	0.91	0.1224

Table 2 — Key parameters and their transformations in Yb-Hf nuclei as ζ surpasses the critical threshold (ζ ~ 0.7), illustrating the disruption and interplay between ζ and nuclear characteristics

Nuclei	N	A	NB	ε=2(NB-1)A [31](keV)	k (keV)	ε/ k = 4NB (1- ζ)/ ζ	ζ = 4NB/(ε/ k)+4NB [24]	(dE4/2*B(E2)↑); e^2b^2
70Yb	88	158	9	2528	109.10	23.17	0.58	0.5440
70Yb	90	160	10	2880	178.10	16.17	0.69	0.7220
70Yb	92	162	11	3240	208.36	15.55	0.72	0.7044
70Yb	94	164	12	3608	221.75	16.27	0.73	0.4416
70Yb	96	166	13	3984	224.45	17.75	0.73	0.1990
70Yb	98	168	14	4368	239.08	18.27	0.74	0.1450
70Yb	100	170	15	4760	197.08	24.00	0.70	0.0460
70Yb	102	172	16	5160	140.33	36.77	0.62	0.0240
72Hf	90	162	9	2592	133.74	19.38	0.65	0.3041
72Hf	92	164	10	2952	151.22	17.14	0.70	0.3257
72Hf	94	168	11	3320	168.01	19.76	0.69	0.4982
72Hf	96	170	12	3696	179.67	20.57	0.70	0.3690
72Hf	98	172	13	4080	159.31	25.61	0.67	0.2759
72Hf	100	174	14	4472	155.06	28.84	0.66	0.0930
72Hf	102	176	15	4872	127.00	38.36	0.61	0.0780

$R6/0 = E(\ ^{+})/E(\ ^{+})$ … (3)

$dE4/2 = E4/2(N)-E4/2(N-2)$ … (4)

In Eq. 4, the first difference of the energy ratio, dE4/2, serves as a sensitive probe of structural evolution, reflecting how the ratio changes with increasing neutron number N. A value of dE4/2 ~ 1 is indicative of a critical point in the shape phase transition—from spherical (U(5)) to deformed (SU(3)) symmetry. It is important to note that the energy ratios are unit less, whereas the individual excitation energies are expressed in keV.

This differential approach enhances the resolution of nuclear structure analysis, capturing abrupt shape changes that are often missed by traditional energy ratios. It provides a more nuanced perspective on nucleonic interactions and sub-shell effects.

When combined with the transition probability B(E2; $0^{+}\rightarrow2^{+}$); e^2b^2, the product dE4/2× B(E2; $0^{+}\rightarrow2^{+}$) becomes a powerful diagnostic tool. The product simultaneously captures spectral rearrangement (via energy derivatives) and collective enhancement (via transition probabilities). Pronounced extrema in this quantity indicate rapid structural reorganization, making it particularly sensitive to critical-point behavior associated with nuclear shape phase transitions. Peaks in this product near N~90 signify enhanced collectivity and rapid structural transitions. Higher values of this parameter indicate strong coupling between nucleonic shape dynamics and collective deformation—a behavior consistent with increased deformation and collectivity.

This composite parameter, with same units of e^2b^2, thus captures both kinematic (energy ratio) and dynamic (transition strength) aspects of nuclear behavior, offering a deeper understanding of symmetry transitions beyond conventional indicators.

3 Results and Discussion

3.1 Gd- Hf Nuclear Sub Region

Figure 3 illustrates the dynamic behavior of the (dE4/2 × B(E2)↑) across the Gd-Er nuclear shell region as a function of the control parameter ζ. This region, especially around Gd, has been extensively studied for its proton and neutron configurations. Prior research[6,7] has thoroughly examined the evolution of Gd isotopes from spherical to deformed shapes. Our results (Fig. 3, left) reveal a prominent peak in dE4/2 × B(E2)↑ for Gd at N= 88 as, ζ increases from 0.4. A notable dip appears near ζ ~ 0.6, corresponding to the critical point nucleus (N ~ 90) indicated with a vertical section. At Z = 64, the sub-shell impact is evident, indicated by a sharp rise (above the unit line) in the systematic behavior at ζ ~ 0.4, especially in[154]Gd. This pattern weakens beyond ζcrit ~ 0.6 (N ~ 90), suggesting a clear structural phase transition—a signature that was less emphasized in previous analyses[6,7]. The recurrence of the critical behavior near ζ ≈ 0.6 across multiple isotopic chains suggests that this threshold is not nucleus-specific but reflects a general structural property of the IBA Hamiltonian.

The Dy and Er isotopic chains exhibit broadly similar systematic behavior; however, in the case of Er isotopes the transition appears to be slightly delayed, with experimental data available primarily at lower excitation energies for N = 86 and more limited information for higher neutron numbers[15]. The entire Gd–Er isotopic chain displays a clear transition from U(5) to SU(3) symmetry around ζ ≈ 0.6, where the corresponding values intersect the unit line on the y-axis. This behavior is further supported[15] by systematic trends observed in the excitation energy ratio $R_{6/0}$, as illustrated in Fig. 3.

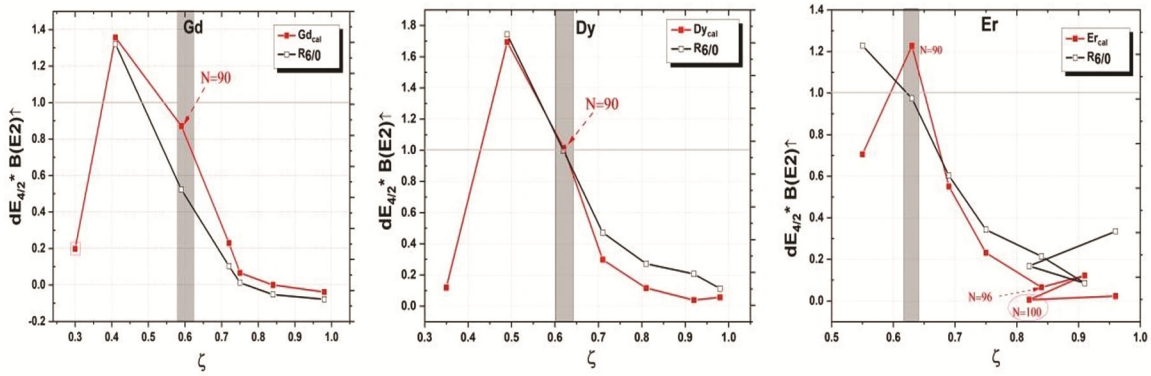

Fig. 3 — The evolution of ($dE_{4/2}$ × B(E2)↑) as a function of ζ for Gd–Er isotopes, showing a clear U(5) to SU(3) transition near ζ_{crit} ~ 0.6. New Er data extend[15] and confirm the robustness of the proposed signature using experimental $R_{6/0}$ values

Notably, the present analysis reveals pronounced kinks in the systematics just prior to N ≈ 90, indicating abrupt structural changes. Such features are consistent with previously reported structural anomalies in this region[20]. The enhanced sensitivity of the refined empirical signature $dE_{4/2} \times B(E2)\uparrow$ enables a more precise identification of nuclear shape transitions compared to earlier approaches. Moreover, plotting ζ against $dE_{4/2} \times B(E2)\uparrow$ yields a nearly universal representation of nuclear collectivity, thereby refining and extending the interpretation of Fig. 2(a)[15].

A detailed comparison between theoretical predictions and experimental data for the Gd–Er isotopic chains is presented in Table 1. For the $^{156-166}$Er isotopes, the present model predicts a critical value of approximately 1.22 at N = 90, which decreases to about 0.06 at N = 96. This behavior reflects a reduction in collectivity as ζ approaches unity, indicating a transition from spherical U(5) to deformed SU(3) symmetry. These results are consistent with earlier investigations, in which both experimental and theoretical P(Z, N) values exhibit a pronounced maximum near N ≈ 90 in $^{154-164}$Er nuclei[30].

A notable change in the energy behavior of the 0_1^+ state in Er isotopes is observed near N ≈ 100, as shown in Fig. 3 (right). This behavior is consistent with earlier reports of anomalous 0_2^+ excited states emerging in this neutron-number region[14]. These observations further support the applicability of Grodzins systematics, in conjunction with the ζ parameter, for reliably tracking nuclear shape transitions within the IBA framework.

Further analysis of the variation of the IBA parameter *ε/k* with neutron number N (Fig. 4) reveals an inverse correlation with the 0^+ energy level, particularly for Gd–Er isotopes with N > 90. This supports the earlier observations of[14], and sharpens their findings by offering a clearer resolution of the shape transition zone.

3.2 Yb-Hf Nuclear Sub Region

The variation of dE4/2 × B(E2)↑ as a function of ζ for Yb–Hf isotopes is presented in Fig. 5. In this sub region, the values remain consistently below unity, while ζ trends toward the SU(3) limit. A notable shift in the energy distribution of the excited 01+ level is observed for Yb at N ~ 100, which is also seen for Hf at the same neutron number (Figs. 2 and 4). This observation is consistent with earlier reports of anomalous 0_2^+ behavior in Yb isotopes[14] near N = 100.

This observation is further supported by analyses in which fluctuations in $dE_{4/2} \times B(E2)\uparrow$ were examined as a function of the valence product N_pN_n for $^{162-176}$Hf isotopes, revealing increasing deformation as N_pN_n approaches 120 (N ≈ 96)[19]. Similar systematic behavior has been reported in studies identifying F-spin multiplets in nuclei extending up to N = 104, well away from the valley of β stability[31]. Additional corroboration of this transition has been obtained through investigations employing the Grodzins relation, which identify a critical point[16] near $P_{crit} \approx 4–5$. As ζ exceeds approximately 0.6, a gradual yet distinct structural evolution becomes evident across the Yb–Hf isotopic chains (Table 2), with the present model successfully reproducing these subtle deformation effects.

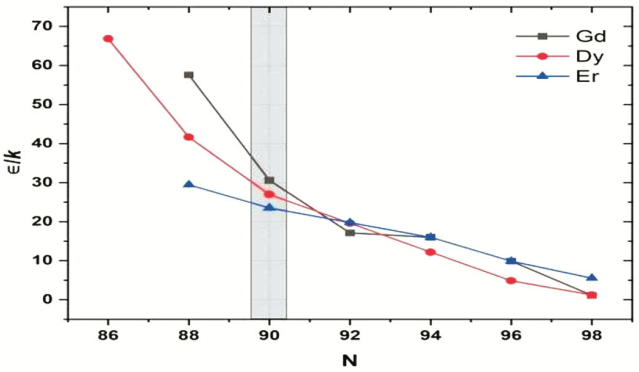

Fig. 4 — ε/κ versus neutron number N illustrating the s–d boson interaction strength in the IBA model. The shaded region near N ≈ 90 marks the onset of shape transitions, where increased ε/κ correlates with lowered 0^+ energies, consistent with the structural phase change reported[32]

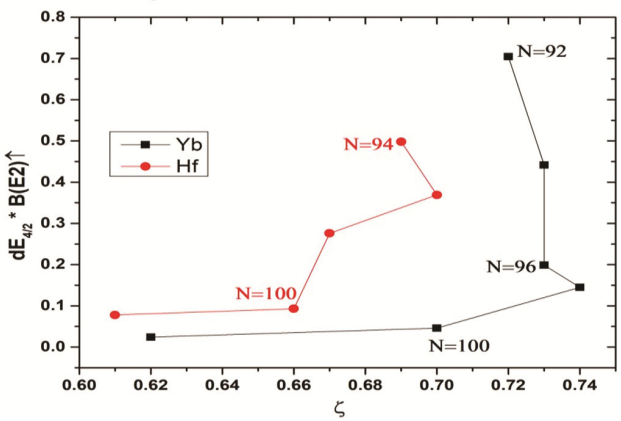

Fig. 5 — Variation of $dE_{4/2} \times B(E2)\uparrow$ with ζ for Yb–Hf isotopes, showing mid-shell anomalies near N ≈ 100 and convergence toward the SU(3) limit. Corresponding ζ and energy-product values are listed in Table 2

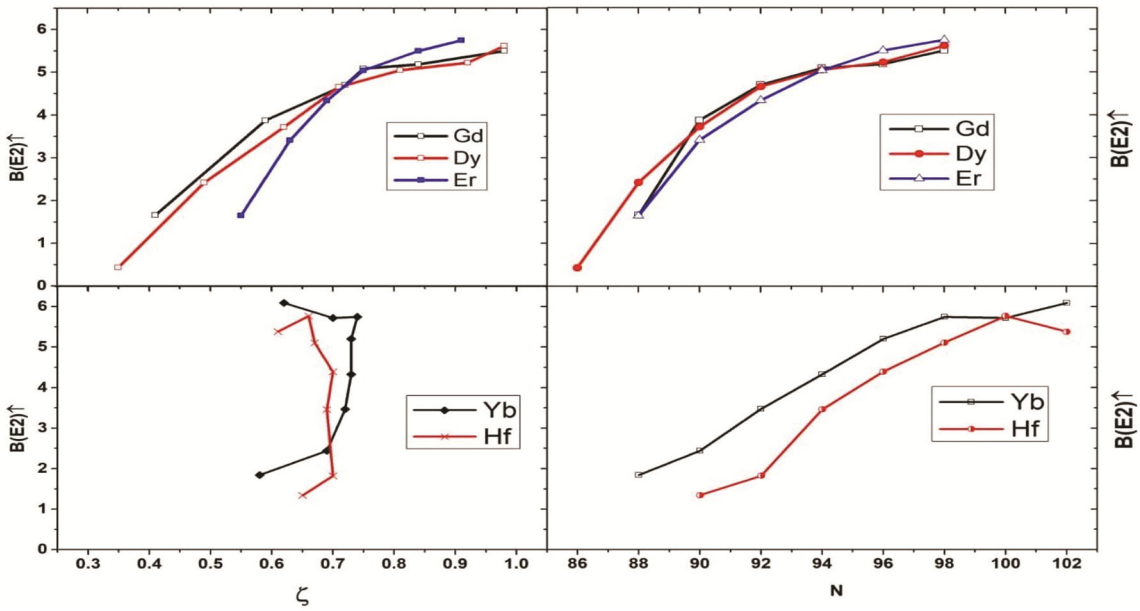

Fig. 6 — Comparison of calculated and experimental B(E2; $0^+ \rightarrow 2^+$) values, showing good agreement and confirming the robustness of the IBA-based description of collectivity across transitional nuclei

The narrow spread in dE4/2 values in Fig. 5 suggests that even small uncertainties in ζ extraction could significantly influence the trend of our signature parameter. However, by combining energy derivatives with collective transition strength data, we achieve a more sensitive diagnostic. The observed sharper kinks and discontinuities compared to[14] demonstrate that our proposed method offers enhanced resolution of structural transitions.

Thus, a revised interpretation of Figs. 2 and 5[14], offering a simplified yet powerful empirical framework for analyzing nuclear shape transitions, while retaining the essential physical insights.

4 Electromagnetic Transition Probability B(E2; $0^+ \rightarrow 2^+$) Characteristics and Symmetry Shifts in Nuclei

The previously described methodology accurately reproduces essential observables—particularly the electromagnetic transition probability B(E2; $0^+ \rightarrow 2^+$), expressed in units of e^2b^2. Figure 6 shows that the computed values closely match experimental trends, confirming the reliability of the IBA-based approach. Analysis of the B(E2)↑ values across nuclei near the U(5)–SU(3) leg of the Casten triangle (IBA symmetry triangle) (Fig. 1) reveals a systematic pattern, reflecting the evolution of axial symmetry[33]. In particular, Gd and Dy isotopes exhibit a rapid transition from spherical to deformed shapes, marked by distinct changes in B(E2)↑, consistent with the predicted symmetry evolution[11]. Our findings not only validate theoretical expectations but also provide empirical confirmation of abrupt symmetry transitions in the rare-earth region. The ability of our refined Grodzins-based parameter to simultaneously track excitation energy ratios and transition probabilities highlights its utility as a diagnostic tool for structural evolution in nuclear systems.

5 Conclusion

This study establishes the product dE4/2 × B(E2)↑ as a robust and intuitive empirical signature for identifying nuclear shape transitions within the Interacting Boson Approximation (IBA) framework. Our analysis demonstrates that a critical threshold at ζ ~ 0.6 marks the transition from spherical U(5) to deformed SU(3) or γ-soft O(6) regimes. This point corresponds to abrupt changes in nuclear collectivity and symmetry structure. Through a systematic investigation of even-even nuclei with Z < 76 and N = 86–102, we identify key structural anomalies in the Gd–Er and Yb–Hf isotopic chains, particularly around N ~ 90–100, suggesting the presence of shape coexistence and mid-shell effects. The present results for Yb–Hf nuclei show significant deviations from earlier modeling approaches that lacked sensitivity to higher-energy behavior and mid-shell anomalies[34]. By integrating Grodzins systematics with the control parameter ζ, this work provides a more refined and interpretable framework for understanding shape

phase transitions—bridging theoretical predictions with experimental observables. The correlation between $B(E2;0^{+}\rightarrow 2^{+})$, $R_{6/0}$, and ζ reinforces the potential of this combined parameter as a predictive and diagnostic tool, offering improved sensitivity over conventional symmetry-based classifications. Owing to its empirical construction and minimal model dependence, the proposed signature can be readily extended to other mass regions where reliable B(E2) data are available, as supported by existing global compilations and our most recent systematic studies of electromagnetic transition strengths[35-39].

References

1 Iachello F, Zamfir N V & Casten R F, *Phys Rev Lett*, 81 (1999) 1191.
2 Casten R F, Kusnezov D & Zamfir N V, *Phys Rev Lett*, 82 (1999) 5000.
3 Casten R F & Zamfir N V, *Phys Rev Lett*, 85 (2000) 3584.
4 Casten R F & Zamfir N V, *Phys Rev Lett*, 85 (2001) 052503.
5 Krücken R *et al*., *Phys Rev Lett*, 88 (2002) 232501.
6 Bizzeti P G & Bizzeti-Sona A M, *Phys Rev C*, 66 (2002) 031301.
7 Tonev D *et al*., *Phys Rev C*, 69 (2004) 034334.
8 Iachello F, *Phys Rev Lett*, 85 (2000) 3580.
9 Iachello F, *Phys Rev Lett*, 87 (2001) 052502.
10 Casten R F & Zamfir N V, *Phys Rev Lett*, 87 (2001) 052503.
11 Iachello F & Zamfir N V, *Phys Rev Lett*, 92 (2004) 212501.
12 Rowe D J, Turner P S & Rosensteel G, *Phys Rev Lett*, 93 (2004) 232502.
13 Zhang Y, Hou Z F & Liu Y X, *Phys Rev C*, 76 (2007) 011305.
14 McCutchan E A, Zamfir N V & Casten R F, *Phys Rev C*, 69 (2004) 064306.
15 Bonatsos D, McCutchan E A, Casten R F & Casperson R J, *Phys Rev Lett*, 100 (2008) 142501.
16 Bindra A & Mittal H M, *Int J Nucl Energy Sci Technol*, 13 (2019) 2.
17 Bindra A & Mittal H M, *Chin Phys C*, 41 (2017) 054102.
18 Bindra A & Mittal H M, *Nucl Phys A*, 975 (2018) 48.
19 Ahmad M & Bindra A, *Int J Nucl Energy Sci Technol*, 16 (2023) 316–324.
20 Prášek A *et al*., *Phys Rev C*, 110 (2024) 024317.
21 Scholten O, Iachello F & Arima A, *Ann Phys (N Y)*, 115 (1978) 325.
22 Lipas P O, Toivonen P & Warner D D, *Phys Lett B*, 155 (1985) 295.
23 Zamfir N V, von Brentano P, Casten R F & Jolie J, *Phys Rev C*, 66 (2002) 021304.
24 Werner V, von Brentano P, Casten R F & Jolie J, *Phys Lett B*, 527 (2002) 55.
25 Casperson R J, *Comput Phys Commun*, 183 (2011) 1029.
26 Pritychenko B, Birch M, Singh B & Horoi M*, Nucl Data Sheets,* 107 (2006) 1.
27 Pritychenko B, McCutchan E and Sonzogni A, *Nucl Data Sheets,* 120 (2014) 232.
28 Pritychenko B, Birch M, Singh B & Horoi M, *Data Nucl Data Tables*, 107 (2016) 1.
29 Dieperink A E L, Scholten O & Iachello F, *Phys Rev Lett*, 44 (1980) 1747.
30 Guo X, Zhao H, Pan F & Draayer J P, *Nucl Phys A*, 1003 (2019) 012.
31 Gupta J B, Mittal H M & Sharma S, *Phys Scr*, 41 (1990) 660.
32 Ahmad M, Bindra A, Sharma P & Dogra V, *Proc DAE Symp Nucl Phys*, 68 (2024).
33 Casten R F, *Nucl Phys A*, 443 (1985) 1.
34 Chou W T, Zamfir N V & Casten R F, *Phys Rev C*, 56 (1997) 829.
35 Ahmad M *et al*., *Proc Int Conf on Electrical Engineering/ Electronics, Computer, Telecommunication and Information Technology (ECTI-CON)*, (2025) 1.
36 Ahmad M *et al*., Proc DAE Symp Nucl Phys, 68 (2024) 215.
37 Ahmad M & Bindra A, *Nucl Phys A*, 1067 (2026) 123288.
38 Ahmad M *et al*., Proc DAE Symp Nucl Phys, 69 (2025) 129.
39 Ahmad M, *Proc DAE Symp Nucl Phys*, 69 (2025) 1421.